Spin-orbit excitons and electronic configuration of the $5d^4$ insulator $Sr_3Ir_2O_7F_2$

Zach Porter [1], Paul M. Sarte,[1] Thorben Petersen [2], Mary H. Upton,[3] Liviu Hozoi,[2] and Stephen D. Wilson[1,*]

[1]*Materials Department, University of California, Santa Barbara, California 93106-5050, USA*
[2]*Institute for Theoretical Solid State Physics, Leibniz-IFW Dresden, Helmholtzstraße 20, D-01069 Dresden, Germany*
[3]*Advanced Photon Source, Argonne National Laboratory, Argonne, Illinois 60439, USA*

Here, we report on the low-energy excitations within the paramagnetic spin-orbit insulator $Sr_3Ir_2O_7F_2$ studied via resonant inelastic x-ray scattering, *ab initio* quantum chemical calculations, and model Hamiltonian simulations. This material is a unique d^4 Ir^{5+} analog of $Sr_3Ir_2O_7$ that forms when F ions are intercalated within the SrO layers spacing the square lattice IrO_6 bilayers of $Sr_3Ir_2O_7$. Due to the large distortions about the Ir^{5+} ions, our computations demonstrate that a large single-ion anisotropy yields an $S = 1$ ($L \approx 1$, $J \approx 0$) ground-state wave function. Weakly coupled, excitonic modes out of the $S_z = 0$ ground state are observed and are well described by a phenomenological spin-orbit exciton model previously developed for $3d$ and $4d$ transition metal ions. The implications of our results regarding the interpretation of previous studies of hole-doped iridates close to d^4 fillings are discussed.

I. INTRODUCTION

A considerable amount of theoretical [1–8] and experimental [9] work has been dedicated to exploring the magnetism of the $J_{eff} = 0$ ground state and its potential for excitonic magnetism. The driving idea is that strong spin-orbit coupling (SOC) native to heavy transition metal ions in high-symmetry crystal field environments can lead to $J_{eff} = 0$ ground states, and the Van Vleck-type spin-orbit excitons that result above this ground state (e.g., $J = 0$ to $J = 1$) can condense into so-called "excitonic" magnetic order [1]. This can engender a quantum critical point with high-energy scale fluctuations [2]. And, for some material realizations, the condensed phase itself may support novel spin-liquid states.

Earlier studies on double perovskite variants have studied nonmagnetic $J_{eff} = 0$ states [10,11]. Yet it is rare to find a materials platform that enables the study of spin-orbit excitonic states upon changing the ground-state wave function from magnetic $J_{eff} = 1/2$ to nonmagnetic $J_{eff} = 0$, all while preserving the lattice topology and metal site ion. Excitingly, recent studies have shown that previously established topochemical transformation techniques and intercalation pathways developed for Ruddelsden-Popper phases in $3d$ and $4d$ transition metal oxides [12,13] can also be leveraged on their $5d$-electron cousins [14,15]. This provides the opportunity to control the oxidation state in $5d^5$ iridates with $J_{eff} = 1/2$ ground states and drive them into $5d^4$ $J_{eff} = 0$ states, while preserving the metal ion character and lattice topology.

Of particular interest is $Sr_3Ir_2O_7F_x$ with $0 \leqslant x \leqslant 2$, a d^5 iridate which can be driven into the d^4 state via fluorine intercalation [14]. This fluorine system presents several ad-

vantages for studying $5d^4$ physics over other modifications to $Sr_3Ir_2O_7$. Previous studies of $Sr_3Ir_2O_7$ when alloyed with $4d^4$ Ru have resolved an anomalous hardening of magnon modes combined with a narrowing of the excitation bandwidth as the $Sr_3Ru_2O_7$ endpoint is approached [16], similar to results for the monolayer analog $Sr_2(Ir, Ru)O_4$ [17]. Resolving a crossover into a pure d^4 excitonic state was prohibited by the diminishing fraction of Ir needed for conventional hard resonant x-ray measurements as well as by the intrinsic disorder broadening native to the Ir/Ru alloying in the system. Single crystals of $Sr_3Ir_2O_7F_2$ potentially provide a unique new window into this problem by circumventing both of these roadblocks.

Here, we present a study of spin-orbit exciton dynamics in the $5d^4$ system $Sr_3Ir_2O_7F_2$. By using resonant inelastic x-ray scattering (RIXS) measurements combined with *ab initio* quantum chemistry calculations and a phenomenological spin-orbit exciton model, we demonstrate that $Sr_3Ir_2O_7F_2$ realizes a spin-orbit singlet $S = 1$ ($L \approx 1$, $J \approx 0$) ground state whose excitation spectrum is governed by the interplay between strong SOC and strong distortions within the local ligand fields about the Ir sites. Weakly coupled spin-orbit excitons and d-d excitations are observed and establish the energy scales of SOC, coupling strengths, and crystal field splitting. The implications for interpreting the anomalous excitation spectrum observed in heavily substituted $Sr_3(Ir_{1-x}Ru_x)_2O_7$ alloys are discussed.

II. EXPERIMENTAL AND COMPUTATIONAL DETAILS

$Sr_3Ir_2O_7F_2$ crystals were prepared using the methods described elsewhere [14]. The exact synthetic conditions and further characterization are described in the Supplemental Material [18]. Resonant inelastic x-ray scattering (RIXS)
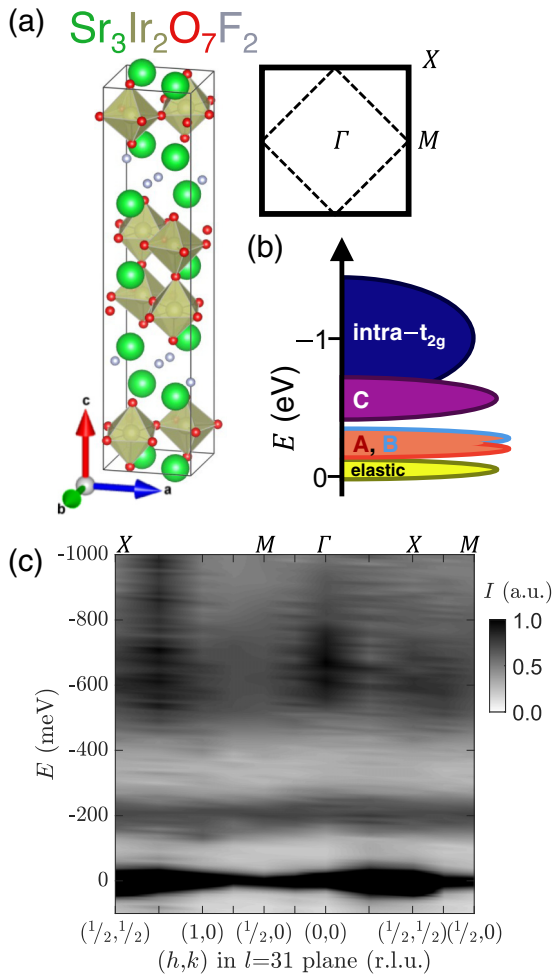
*stephendwilson@ucsb.edu

FIG. 1. (a) Orthorhombic *Bbcb* unit cell (left) and quasi-2D Brillouin zone (right) for $Sr_3Ir_2O_7F_2$. Ir-O bond lengths are appreciably compressed along c near the fluorine planes. (b) Illustration of the excitations observed in RIXS measurements. Details are in the text. (c) RIXS false-color map of raw intensities in the quasi-2D Brillouin zone. Ticks indicate the **Q** positions where spectra were measured, and the map was generated by interpolation.

measurements were performed at 8 K on Beamline 27-ID-B of the Advanced Photon Source at Argonne National Laboratory. The incident photons were tuned to the Ir L_3 absorption edge ($E = 11.215$ keV) and final energies were selected with the Si (4,4,8) reflection of a spherical analyzer crystal array in a horizontal scattering geometry [19]. Excitations were mapped primarily in the quasi-two-dimensional (2D) $l = 31$ Brillouin zone (BZ) with an energy resolution ≈35 meV. This l value was chosen because it is far from Bragg peaks and near $2\theta = 90°$ where Thomson scattering (i.e., elastic charge scattering) is minimized. Momentum space positions are indexed using an orthorhombic *Bbcb* unit cell with lattice parameters $a = 5.45$ Å, $b = 5.51$ Å, and $c = 24.21$ Å; see Fig. 1. This simplification from the proper $C2/c$ cell was chosen for comparison to other quasi-2D perovskite variants. Due to twin structural domains, we do not distinguish between a and b axes.

Ab initio quantum chemical calculations were performed on both single-octahedron $[IrO_6]^{7-}$ and two-octahedra $[Ir_2O_{11}]^{12-}$ clusters [18], embedded in point charge fields (PCFs) created by using experimentally determined lattice positions [14] as input for the EWALD program [20,21]. Excited state energies were calculated on the basis of *ab initio* complete active space self-consistent field (CASSCF) theory [22,23], considering the Ir t_{2g} atomic orbitals in active spaces of the sizes CAS(4e,3o) and CAS(8e,6o) for single-octahedron and two-octahedra clusters, respectively. Subsequently, dynamical correlation was treated in the scheme of the multireference configuration interaction (MRCI), with the Ir $4f$, Ir $5s$, Ir $5p$, and O $2p$ orbitals correlated in the CI part. All calculations were performed with the program package ORCA version 5.0 [24] and further details are in the Supplemental Material [18].

III. RESULTS

Looking first at Fig. 1, the structure of $Sr_3Ir_2O_7F_2$ is shown in Fig. 1(a). IrO_6 octahedra are asymmetrically compressed, with the O ions closest to intercalated F ions pushed inward toward the Ir ions. Figure 1(b) provides a qualitative illustration of the spectral features and relative energy scales probed by RIXS measurements at the Ir L_3 edge in $Sr_3Ir_2O_7F_2$, and Fig. 1(c) shows a momentum-energy transfer map of RIXS intensities measured across the quasi-2D Brillouin zone.

All modes observed are weakly dispersive, and we label the features as elastic at energy loss $E = 0$ meV, A at $E \approx 170$ meV, B at $E \approx 220$ meV, and C at $E \approx 500$–900 meV. A, B, and C are spin-orbit excitons. A representative fit parametrizing these features is shown in Fig. 2(a), where the elastic line was fit to a Voigt function, peaks A and B were fit to Lorentzians, and other features were empirically fit to Gaussians. The key features parametrized within this spectrum are the A and B peaks, which we will demonstrate are spin-orbit excitons out of the $S = 1$, $J = 0$ ground state.

An important first step is to demonstrate the presence of two distinct exciton modes near 200 meV, which are nominally split by the large, noncubic distortion of the IrO_6 octahedra. Figure 2(b) shows the RIXS spectra about this energy region at the 2D zone center with varying l values. Changing the value of l modulates the intensities of the A and B modes; mode A can be mostly isolated at $l = 32$ and mode B at $l = 29$. The integrated intensities of the A and B modes are plotted as a function of l in Fig. 2(c), where the intensity of the A mode is well described by the form $\sin^2(\pi l d/c)$, with d being the bilayer Ir-Ir spacing and c being the lattice constant. For the B mode, the modulation of the intensity is $\pi/2$ out of phase with an added constant background. We attribute this sinusoidal behavior of A and B to a double-slit-like interference for two different excited states that are delocalized across the bilayer. This interference effect results from the emission process in RIXS, [26], and was invoked to explain the scattering for $Sr_3Ir_2O_7$ [27] and for dimer compounds such as $Ba_3CeIr_2O_9$ [28,29]. A more detailed description of the physical origin and alternative explanations are provided in the Supplemental Material [18].
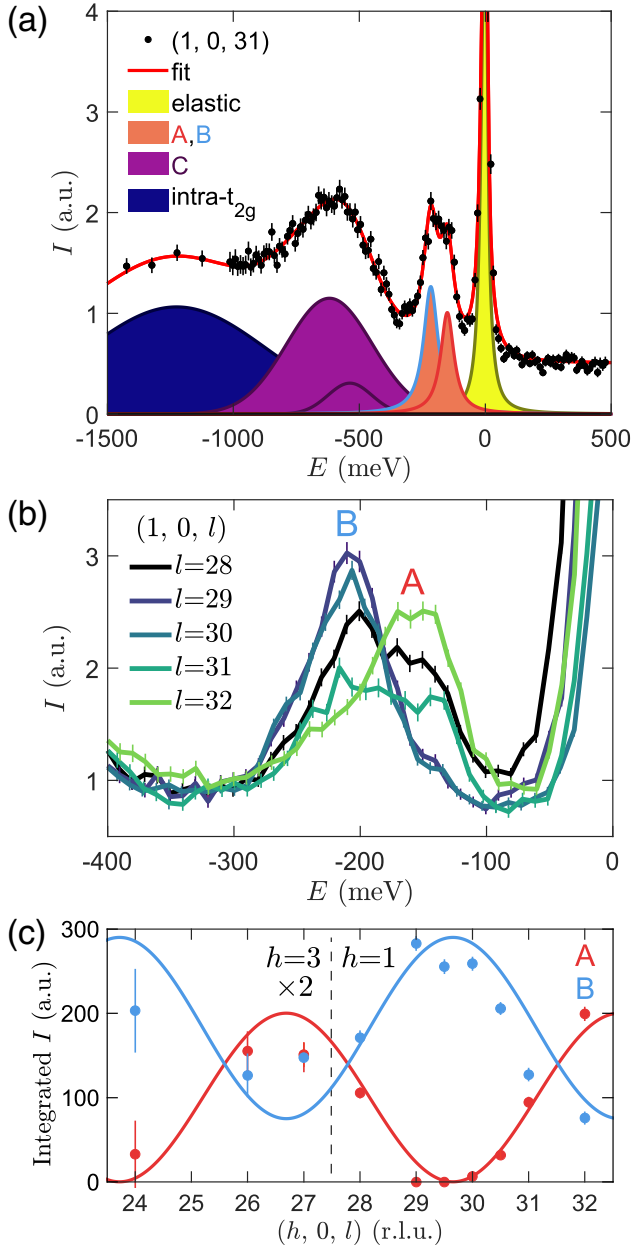
FIG. 2. (a) Representative RIXS spectrum (black dots) collected at $\mathbf{Q} = (1, 0, 31)$. Fits to the spectra (solid red lines) utilize the spectral components discussed in the text in addition to a constant background term. (b) Raw RIXS spectra at $(1, 0, l)$ show the change in spectral weight of the A and B features (red and blue, respectively). (c) Integrated intensities of the Lorentzian fits to these features reveal sinusoidal dependence in l. The functional form of the red line is $\sin^2(\pi l d/c)$, as is described in the text. Note that for $l \leqslant 27$ the fitted scans were measured at $(3, 0, l)$. This scattering geometry has longer scattering path lengths, and greater self-absorption. Thus the $h = 3$ scans were scaled by a factor of 2 to make the intensity values comparable, following Ref. [25].

A. Phenomenological Model

The energies of the peaks A and B can be determined under fixed l and plotted across the 2D zone, and the resulting dispersion and level spacing is shown in Fig. 3. Assuming weak
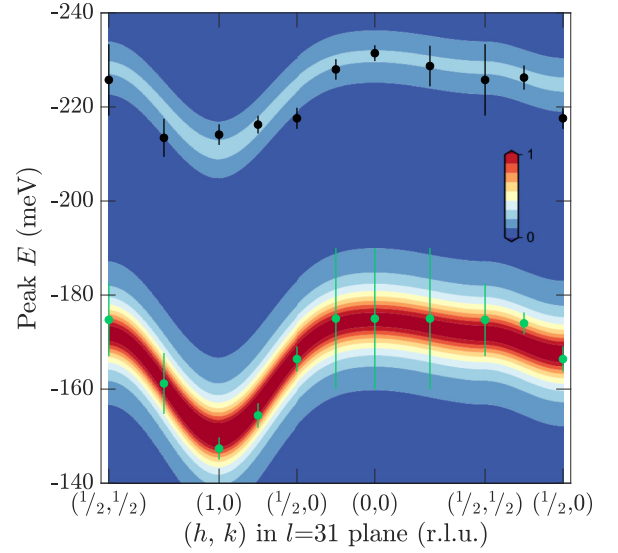

FIG. 3. Spin-orbit exciton model (solid colors and lines) in comparison to the fitted data (points). Energy transfers of transverse (lower-energy) and longitudinal (higher-energy) modes overplotted on $S(\mathbf{Q})$. Note that the RIXS intensity is not equivalent to $S(\mathbf{Q})$, and intensities have not been scaled to account for the scattering geometry. Error bars only account for peak energy uncertainty, and do not incorporate fixed widths ≈ 60 meV.

correlations between bilayers similar to $Sr_3Ir_2O_7$ [30], this quasi-2D dispersion can then be phenomenologically fit via a square lattice spin-orbit exciton model assuming an idealized $S = 1$ ($L = 1$, $J = 0$) ground state and a single-ion Hamiltonian $\hat{\mathcal{H}}_{SI}$. This model for $Sr_3Ir_2O_7F_2$ employs the same formalism that was established [31] for the d^4 multiorbital Mott insulator Ca_2RuO_4. This Hamiltonian is parametrized by $\alpha'\lambda$, H_{MF}, and δ, corresponding to the individual contributions from spin-orbit coupling (with the prefactor $\alpha' = 1/2$), an internal mean molecular field, and a uniaxial (either tetragonal or trigonal) distortion of the local octahedral coordination environment, respectively. The resulting eigenstates of $\hat{\mathcal{H}}_{SI}$ are then coupled by the Fourier transform of the exchange interaction $J(\mathbf{Q})$, where both an isotropic nearest-neighbor J_1 and next-nearest-neighbor exchange J_2 are considered [18].

The refined parameters from this model are shown in Table I, and the model's results are overplotted with the experimental data points in Fig. 3. Two distinct modes are parametrized with calculated dispersion relations in excellent agreement with the experimental data. The lower-energy A mode corresponds to transverse fluctuations ($\alpha\beta = +-$ and

TABLE I. Refined parameter values of the spin-orbit exciton model for $Sr_3Ir_2O_7F_2$. All values are reported in meV.

Parameter	Initial value	Range	Refined value
λ	400	[300, 500]	374
H_{MF}	0	[−5, 5]	0.2
δ	80	[40, 120]	100
J_1	2	[0, 5]	2.1
J_2	−1	[−2, 2]	−0.8

TABLE II. Ir^{5+} $5d^4$ multiplet structure, MRCI (without and with SOC), and RIXS relative energies, all in meV, for an embedded $[IrO_6]^{7-}$ octahedron using experimental crystallographic data. Notations reference cubic symmetry, even though the actual symmetry is much lower; for this reason, T and E crystal field states (second column) are split up.

Ir^{5+} t_{2g}^4 terms	MRCI	MRCI+SOC	RIXS	Assignment
$^3T_{1g}$	0	0 ($J \approx 0$)	0	Elastic ($S_z = 0$)
	106	290, 370 ($J \approx 1$)	170, 210	A, B ($S_z = \pm 1$)
	324	500 ($J \approx 1$)	≈ 550	C
		720, 740, 760, 800, 870 ($J \approx 2$)	≈ 750	C
$^1T_{2g}$, ^1E_g	876, 896, 1013, 1235, 1341	1570, 1610, 1680, 1846, 1946 ($J \approx 2$)	>1000	Intra-t_{2g}
$^1A_{1g}$	2396	3102		

$-+$) within the basal plane of the pseudotetragonal unit cell, whereas the B mode at higher-energy transfers corresponds to longitudinal zz fluctuations along the Ir^{5+} moment's axis.

We now describe the quantitative results of the spin-orbit exciton model, with modeled uncertainties indicated in parentheses. The refined value of 374(10) meV for the spin-orbit coupling λ is comparable to values reported for other d^4 iridates [10,11]. The presence of one, rather than two, transverse modes can be understood by the negligible molecular field. According to the model, H_{MF} has a refined value of 0.2(2) meV, and this implies no splitting between the two plausible $\alpha\beta = +-$ and $-+$ transverse modes. The lack of a molecular field is also consistent with the absence of magnetic long-range order in this material. In such a case where the molecular field is absent, the gap between the longitudinal and transverse modes can be modeled via a uniaxial distortion of the coordination environment for a magnetic ion with unquenched orbital angular momentum. The large magnitude of δ with a refined value of 100(5) meV yields a significant gap of $\delta/2$. The weak dispersion is captured by a weak antiferromagnetic $J_1 > 0$ and ferromagnetic $J_2 < 0$. This model parametrizes these two lowest-energy A and B excitations as transverse and longitudinal $S = 1$ exciton branches, split by a strong tetragonal distortion, with negligible molecular field. This minimal phenomenological model captures the dispersion with only weak in-plane coupling, and any potential effects due to out-of-plane couplings and how to differentiate them from the interference effects in RIXS are not addressed.

B. *Ab Initio* Calculations

The spin-orbit exciton model described above assumes a simplified, uniform tetragonal distortion, which is not the case for $Sr_3Ir_2O_7F_2$. As a complementary computational approach to the $5d$ electronic structure, quantum chemical calculations were carried out; see Table II. These *ab initio* results indicate strong low-symmetry fields, comparable to the magnitude of SOC. The computed spin-orbit ground-state wave function features dominant in-plane orbital occupation and we confirm that the first two excited states essentially correspond to $S_z = \pm 1$, although their relative energy is overestimated in the quantum chemical treatment. Another distinct level is found near 500 meV. Without SOC, the lowest $S = 0$ (t_{2g}^4) states are computed at ≈ 1 eV (second column in Table II). Spin-orbit interactions push those levels to higher energies (third column in Table:II), but these effects might be overestimated in the computations since higher-lying $t_{2g}^3 e_g^1$ terms and O-to-Ir

charge-transfer states are not included in the CAS treatment. As an approximation, additionally including the unoccupied e_g atomic orbitals in the CAS treatment did not result in a closer agreement [18].

Despite overestimating the energy range of the $S_z = \pm 1$ modes, the *ab initio* data describe the RIXS spectrum qualitatively quite well. Most importantly, the energy splitting of the A and B modes modeled in the phenomenological spin-orbit exciton model is captured and the higher-energy electronic transitions are identified. The A and B features in the RIXS spectrum can then be analyzed in terms of intramultiplet spin-orbit exciton modes within the group of $S = 1$ ($J \approx 0$ and $J \approx 1$) states.

The full width at half maxima (FWHM) of the A and B exciton modes are reasonably narrow (60 meV), close to the experimental resolution (35 meV), allowing for a reliable extraction of the effective bandwidth: 15–35 meV. Quantum chemical calculations of the $[Ir_2O_{11}]^{12-}$ embedded cluster model reveal that each of these modes is split by about 10 meV. This is consistent with the dispersion arising from the exchange coupling. The C feature has FWHM values near 100 meV, and a bandwidth of about 80 meV, reminiscent of the broad spin-orbit excitons identified for Sr_2IrO_4 [32] and $Sr_3Ir_2O_7$ [30].

IV. DISCUSSION AND CONCLUSIONS

Having established that $Sr_3Ir_2O_7F_2$ provides a platform for the direct resolution of spin-orbit exciton modes in a d^4 iridate bilayer, it allows analysis of the anomalous excitation spectra previously reported in the $Sr_3(Ir_{1-x}Ru_x)_2O_7$ system. Prior studies reported an unusual hardening of the magnetic excitation gap upon hole doping and the persistence of robust antiferromagnetic spin fluctuations up to dopings as high as $x = 0.77$ in the Ruddlesden-Popper series strontium iridates [16,17]. The excitation bandwidth correspondingly narrows and localizes to ≈ 200 meV, the regime where the $S_z = \pm 1$ modes are observed in $Sr_3Ir_2O_7F_2$.

Prior models leveraged local exchange disorder or coupling to the particle-hole continuum to explain the anomalous excitation spectra of $Sr_3(Ir_{1-x}Ru_x)_2O_7$; however, our resolution of the purely excitonic spectrum of $Sr_3Ir_2O_7F_2$ should map to the d^4 endpoint of $Sr_3(Ir_{1-x}Ru_x)_2O_7$. Our findings suggest that local d^4 iridium sites in the electronically inhomogeneous iridate-ruthenate alloy [33] likely drive the apparent gap hardening. The lifetimes of low-energy excitations in $Sr_3(Ir_{1-x}Ru_x)_2O_7$ are exceptionally broad, and as the mag-

netic moment collapses with hole doping upon entering the metallic regime, the local spin-orbit excitons endemic to d^4 sites dominate the RIXS spectrum.

$Sr_3Ir_2O_7$ itself has recently been proposed to be an excitonic insulator with an antiferromagnetic ground state [27], and $Sr_3Ir_2O_7F_2$ provides an important nonmagnetic $J = 0$ comparator for understanding how the local electronic structure and interactions evolve as holes are introduced into the compound. Our RIXS data combined with quantum chemistry calculations and a phenomenological spin-orbit exciton model allow us to identify the effective spin-orbit coupling, tetragonal distortion, and exchange coupling energies in a unique, d^4 Ruddelsden-Popper bilayer iridate.

ACKNOWLEDGMENTS

[1] G. Khaliullin, Phys. Rev. Lett. **111**, 197201 (2013).

[2] O. N. Meetei, W. S. Cole, M. Randeria, and N. Trivedi, Phys. Rev. B **91**, 054412 (2015).

[3] J. Kuneš, J. Phys.: Condens. Matter **27**, 333201 (2015).

[4] S. Bhowal, S. Baidya, I. Dasgupta, and T. Saha-Dasgupta, Phys. Rev. B **92**, 121113(R) (2015).

[5] J. Chaloupka and G. Khaliullin, Phys. Rev. Lett. **116**, 017203 (2016).

[6] C. Svoboda, M. Randeria, and N. Trivedi, Phys. Rev. B **95**, 014409 (2017).

[7] B. J. Kim and G. Khaliullin, Phys. Rev. B **96**, 085108 (2017).

[8] D. Geffroy, J. Kaufmann, A. Hariki, P. Gunacker, A. Hausoel, and J. Kuneš, Phys. Rev. Lett. **122**, 127601 (2019).

[9] For an experimental review, see Ref. [34]. Some more recent examples are Refs. [11,35,36].

[10] B. Yuan, J. P. Clancy, A. M. Cook, C. M. Thompson, J. Greedan, G. Cao, B. C. Jeon, T. W. Noh, M. H. Upton, D. Casa, T. Gog, A. Paramekanti, and Y. J. Kim, Phys. Rev. B **95**, 235114 (2017).

[11] M. Kusch, V. M. Katukuri, N. A. Bogdanov, B. Büchner, T. Dey, D. V. Efremov, J. E. Hamann-Borrero, B. H. Kim, M. Krisch, A. Maljuk, M. M. Sala, S. Wurmehl, G. Aslan-Cansever, M. Sturza, L. Hozoi, J. van den Brink, and J. Geck, Phys. Rev. B **97**, 064421 (2018).

[12] R. Zhang, M. S. Senn, and M. A. Hayward, Chem. Mater. **28**, 8399 (2016).

[13] R. K. Li and C. Greaves, Phys. Rev. B **62**, 3811 (2000).

[14] C. Peterson, M. W. Swift, Z. Porter, R. J. Clément, G. Wu, G. H. Ahn, S. J. Moon, B. C. Chakoumakos, J. P. C. Ruff, H. Cao, C. Van de Walle, and S. D. Wilson, Phys. Rev. B **98**, 155128 (2018).

[15] K. Kuramochi, T. Shimano, T. Nishio, H. Okabe, A. Koda, K. Horigane, J. Akimitsu, and H. Ogino, Phys. Rev. Mater. **4**, 013403 (2020).

[16] J. L. Schmehr, T. R. Mion, Z. Porter, M. Aling, H. Cao, M. H. Upton, Z. Islam, R. H. He, R. Sensarma, N. Trivedi, and S. D. Wilson, Phys. Rev. Lett. **122**, 157201 (2019).

[17] Y. Cao, X. Liu, W. Xu, W. G. Yin, D. Meyers, J. Kim, D. Casa, M. H. Upton, T. Gog, T. Berlijn, G. Alvarez, S. Yuan, J. Terzic, J. M. Tranquada, J. P. Hill, G. Cao, R. M. Konik, and M. P. M. Dean, Phys. Rev. B **95**, 121103(R) (2017).

[18] See Supplemental Material at http://link.aps.org/supplemental/10.1103/PhysRevB.106.115140 for details about sample synthesis and characterization, experimental fits, models, and discussion of the intensity dependence along *l*, which includes Refs. [37–64].

[19] Yu. V. Shvyd'ko, J. P. Hill, C. A. Burns, D. S. Coburn, B. Brajuskovic, D. Casa, K. Goetze, T. Gog, R. Khachatryan, J.-H. Kim *et al.*, J. Electron Spectrosc. Relat. Phenom. **188**, 140 (2013).

[20] S. E. Derenzo, M. K. Klintenberg, and M. J. Weber, J. Chem. Phys. **112**, 2074 (2000).

[21] M. Klintenberg, S. Derenzo, and M. Weber, Comput. Phys. Commun. **131**, 120 (2000).

[22] B. O. Roos, The complete active space self-consistent field method and its applications in electronic structure calculations, in *Ab Initio Methods in Quantum Chemistry Part 2,* edited by K. P. Lawley, Advances in Chemical Physics Vol. 69 (Wiley, New York, 1987), pp. 399–445..

[23] T. Helgaker, P. Jørgensen, and J. Olsen, *Molecular Electronic-Structure Theory* (Wiley-VCH, Chichester, 2000).

[24] F. Neese, WIREs Comput. Mol. Sci. **12**, e1606 (2022).

[25] M. Minola, G. Dellea, H. Gretarsson, Y. Y. Peng, Y. Lu, J. Porras, T. Loew, F. Yakhou, N. B. Brookes, Y. B. Huang, J. Pelliciari, T. Schmitt, G. Ghiringhelli, B. Keimer, L. Braicovich, and M. Le Tacon, Phys. Rev. Lett. **114**, 217003 (2015).

[26] Y. Ma and M. Blume, Rev. Sci. Instrum. **66**, 1543 (1995).

[27] D. Mazzone, Y. Shen, H. Suwa, G. Fabbris, J. Yang, S.-S. Zhang, H. Miao, J. Sears, K. Jia, Y. Shi, M. Upton, D. Casa, X. Liu, J. Liu, C. Batista, and M. Dean, Nat. Commun. **13**, 913 (2022).

[28] A. Revelli, M. Moretti Sala, G. Monaco, P. Becker, L. Bohatý, M. Hermanns, T. C. Koethe, T. Fröhlich, P. Warzanowski, T. Lorenz, S. V. Streltsov, P. H. van Loosdrecht, D. I. Khomskii, J. van den Brink, and M. Grüninger, Sci. Adv. **5**, eaav4020 (2019).

[29] Y. Wang, R. Wang, J. Kim, M. H. Upton, D. Casa, T. Gog, G. Cao, G. Kotliar, M. P. M. Dean, and X. Liu, Phys. Rev. Lett. **122**, 106401 (2019).

[30] J. Kim, A. H. Said, D. Casa, M. H. Upton, T. Gog, M. Daghofer, G. Jackeli, J. van den Brink, G. Khaliullin, and B. J. Kim, Phys. Rev. Lett. **109**, 157402 (2012).

[31] P. M. Sarte, C. Stock, B. R. Ortiz, K. H. Hong, and S. D. Wilson, Phys. Rev. B **102**, 245119 (2020).

[32] J. Kim, D. Casa, M. H. Upton, T. Gog, Y. J. Kim, J. F. Mitchell, M. van Veenendaal, M. Daghofer, J. van den Brink, G. Khaliullin, and B. J. Kim, Phys. Rev. Lett. **108**, 177003 (2012).

[33] C. Dhital, T. Hogan, W. Zhou, X. Chen, Z. Ren, M. Pokharel, Y. Okada, M. Heine, W. Tian, Z. Yamani, C. Opeil, J. S. Helton, J. W. Lynn, Z. Wang, V. Madhavan, and S. D. Wilson, Nat. Commun. **5**, 3377 (2014).

[34] G. Cao and P. Schlottmann, Rep. Prog. Phys. **81**, 042502 (2018).

[35] N. R. Davies, C. V. Topping, H. Jacobsen, A. J. Princep, F. K. K. Kirschner, M. C. Rahn, M. Bristow, J. G. Vale, I. da Silva, P. J. Baker, C. J. Sahle, Y. F. Guo, D. Y. Yan, Y. G. Shi, S. J. Blundell, D. F. McMorrow, and A. T. Boothroyd, Phys. Rev. B **99**, 174442 (2019).

[36] H. Takahashi, H. Suzuki, J. Bertinshaw, S. Bette, C. Mühle, J. Nuss, R. Dinnebier, A. Yaresko, G. Khaliullin, H. Gretarsson, T. Takayama, H. Takagi, and B. Keimer, Phys. Rev. Lett. **127**, 227201 (2021).

[37] N. Fairley, V. Fernandez, M. Richard-Plouet, C. Guillot-Deudon, J. Walton, E. Smith, D. Flahaut, M. Greiner, M. Biesinger, S. Tougaard *et al.*, Appl. Surf. Sci. Adv. **5**, 100112 (2021).

[38] L. Hozoi, A. H. de Vries, A. B. van Oosten, R. Broer, J. Cabrero, and C. de Graaf, Phys. Rev. Lett. **89**, 076407 (2002).

[39] J. Weber and J. Schmedt auf der Günne, Phys. Chem. Chem. Phys. **12**, 583 (2010).

[40] D. Maganas, M. Roemelt, M. Hävecker, A. Trunschke, A. Knop-Gericke, R. Schlögl, and F. Neese, Phys. Chem. Chem. Phys. **15**, 7260 (2013).

[41] D. Aravena, M. Atanasov, and F. Neese, Inorg. Chem. **55**, 4457 (2016).

[42] A. Dittmer, R. Izsák, F. Neese, and D. Maganas, Inorg. Chem. **58**, 9303 (2019).

[43] M. Kaupp, P. v. R. Schleyer, H. Stoll, and H. Preuss, J. Chem. Phys. **94**, 1360 (1991).

[44] D. Andrae, U. Häußermann, and M. Dolg, Theor. Chim. Acta **77**, 123 (1990).

[45] D. A. Pantazis, X.-Y. Chen, C. R. Landis, and F. Neese, J. Chem. Theory Comput. **4**, 908 (2008).

[46] F. Weigend and R. Ahlrichs, Phys. Chem. Chem. Phys. **7**, 3297 (2005).

[47] C. Kollmar, K. Sivalingam, B. Helmich-Paris, C. Angeli, and F. Neese, J. Comput. Chem. **40**, 1463 (2019).

[48] G. L. Stoychev, A. A. Auer, and F. Neese, J. Chem. Theory Comput. **13**, 554 (2017).

[49] M. Douglas and N. M. Kroll, Ann. Phys. **82**, 89 (1974).

[50] B. A. Hess, Phys. Rev. A **33**, 3742 (1986).

[51] W. J. L. Buyers, T. M. Holden, and A. Perreault, Phys. Rev. B **11**, 266 (1975).

[52] P. M. Sarte, M. Songvilay, E. Pachoud, R. A. Ewings, C. D. Frost, D. Prabhakaran, K. H. Hong, A. J. Browne, Z. Yamani, J. P. Attfield, E. E. Rodriguez, S. D. Wilson, and C. Stock, Phys. Rev. B **100**, 075143 (2019).

[53] J. S. Griffith, Trans. Faraday Soc. **56**, 193 (1960).

[54] W. Moffitt, G. L. Goodman, M. Fred, and B. Weinstock, Mol. Phys. **2**, 109 (1959).

[55] U. Walter, J. Phys. Chem. Solids **45**, 401 (1984).

[56] F. Wallington, A. M. Arevalo-Lopez, J. W. Taylor, J. R. Stewart, V. Garcia-Sakai, J. P. Attfield, and C. Stock, Phys. Rev. B **92**, 125116 (2015).

[57] T. Hogan, L. Bjaalie, L. Zhao, C. Belvin, X. Wang, C. G. Van de Walle, D. Hsieh, and S. D. Wilson, Phys. Rev. B **93**, 134110 (2016).

[58] M. Braden, G. André, S. Nakatsuji, and Y. Maeno, Phys. Rev. B **58**, 847 (1998).

[59] L. Das, F. Forte, R. Fittipaldi, C. G. Fatuzzo, V. Granata, O. Ivashko, M. Horio, F. Schindler, M. Dantz, Y. Tseng, D. E. McNally, H. M. Rønnow, W. Wan, N. B. Christensen, J. Pelliciari, P. Olalde-Velasco, N. Kikugawa, T. Neupert, A. Vecchione, T. Schmitt *et al.*, Phys. Rev. X **8**, 011048 (2018).

[60] H. Gretarsson, H. Suzuki, H. Kim, K. Ueda, M. Krautloher, B. J. Kim, H. Yavaş, G. Khaliullin, and B. Keimer, Phys. Rev. B **100**, 045123 (2019).

[61] L. J. P. Ament, G. Khaliullin, and J. van den Brink, Phys. Rev. B **84**, 020403(R) (2011).

[62] J. Jeanneau, P. Toulemonde, G. Remenyi, A. Sulpice, C. Colin, V. Nassif, E. Suard, E. Salas Colera, G. R. Castro, F. Gay, C. Urdaniz, R. Weht, C. Fevrier, A. Ralko, C. Lacroix, A. A. Aligia, and M. Núñez-Regueiro, Phys. Rev. Lett. **118**, 207207 (2017).

[63] D. Reznik, P. Bourges, H. F. Fong, L. P. Regnault, J. Bossy, C. Vettier, D. L. Milius, I. A. Aksay, and B. Keimer, Phys. Rev. B **53**, R14741 (1996).

[64] T. G. Perring, D. T. Adroja, G. Chaboussant, G. Aeppli, T. Kimura, and Y. Tokura, Phys. Rev. Lett. **87**, 217201 (2001).